

WIDEBAND LNA USING A NEGATIVE g_m CELL FOR IMPROVEMENT OF LINEARITY AND NOISE FIGURE

J. Yoon, H. Seo, I. Choi, and B. Kim

Department of Electrical Engineering
Pohang University of Science and Technology
San 31, Hyoja-dong, Nam-gu, Pohang, Gyeongbuk, 790-784
Republic of Korea

Abstract—A differential common gate low noise amplifier (LNA) has been widely used for a wideband LNA. However, it has poor linearity due to a nonlinear transconductance in a MOSFET and poor noise performances from the common gate configuration. We propose a differential common gate LNA with a negative g_m cell for the improvement of the linearity and noise figure. The cell comprises cross coupled transistors instead of a current source. The negative g_m cell creates the opposite phased harmonic, canceling the distortion. The noise figure is improved by canceling the noise from the common gate transistors through the negative g_m cell. The LNA is fabricated in 0.13 μm RF CMOS. The LNA has the bandwidth of 0.7 ~ 3.5 GHz frequency and has provided the expected characteristics for linearity and noise figure.

1. INTRODUCTION

As the wireless communication technology has been rapidly developed, many kinds of mobile communication devices have been introduced in our daily life. For the system, it is highly desirable to integrate the various functions on a single chip due to low cost and low power consumption. For the multiband operation, the conventional systems have employed several parallel narrowband receivers, but it is a high cost solution with high pin count and large chip area. Therefore, research for the multiband receiver has been focusing on the tunable receiver [1, 2]. It requires a tunable LNA or wideband LNA, as the first amplifying stage in the system [3–9].

Corresponding author: J. Yoon (yjh7605@postech.ac.kr).

A common gate (CG) LNA is a widely used topology for the system. It can improve not only the reverse isolation, but also reduce Miller effect [10]. Input impedance of a CG LNA is given by $1/g_m$, which can be adjusted by the bias current, size of the transistor, and overdrive voltage. Therefore, it ($1/g_m$) can be easily matched to the termination impedance across a broad bandwidth. Even though the wideband LNA should satisfy the wide input matching and sufficient gain to overcome the noise of the subsequent stage, the linearity and noise performances are also very important characteristics. Among various distortions, even order distortion can be reduced by exploiting a differential signal processing structure. Therefore, the differential common gate (DCG) LNA, shown in Fig. 1, is the ideal choice for the sufficiently wide input matching, achieved through size optimization of the common gate transistor, and the higher second order intercept point (IIP2) enabled by the even harmonic cancelation [11]. The differential common gate LNA has still a poor third order distortion (IIP3) and high noise performance [12, 13]. We propose the wideband LNA with a negative g_m cell for improvement of the third order distortion in DCG LNA. The LNA depicted in Fig. 2 employs the negative g_m cell instead of the commonly used current source. Since the input impedance of the CG stage is $1/g_m$ and that of the negative g_m cell is $-1/g_m$, g_m coefficients from the two cells can be canceled, linearizing the LNA.

Among the various noise sources in the DCG LNA, thermal noise from the transistor of the CG stage is the most important noise

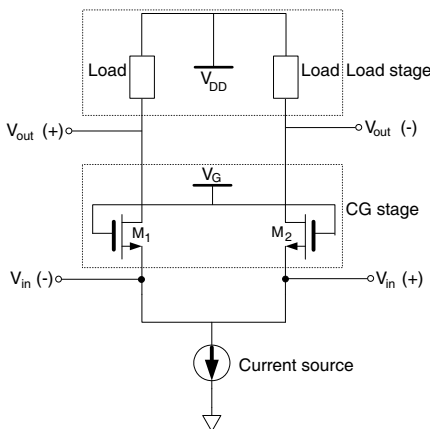


Figure 1. Differential common gate LNA.

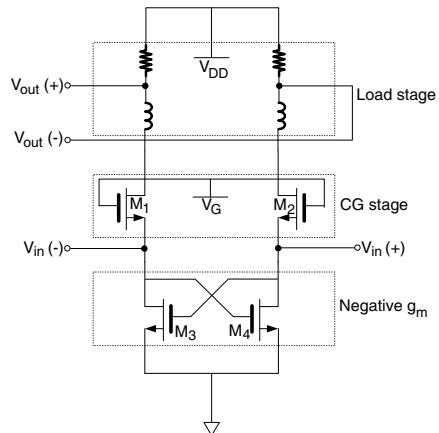


Figure 2. Proposed differential CG LNA with negative g_m cell.

source [14, 15]. The thermal noise from the CG stage is directly delivered to the differential outputs in the conventional DCG LNA. However, in the proposed LNA, a part of the noise is amplified by the negative g_m cell and delivered to the output. The correlated two output noises can be canceled, lowering the noise [9, 16]. In order to demonstrate the improved performances, we have designed the DCG LNA with the negative g_m cell. The LNA demonstrates the expected linearity and noise figure performances. In this paper, we describe the DCG LNA with and without the negative g_m cell in Section 2. In Section 3, we describe the measured results and give conclusions in Section 4.

2. IMPROVEMENT OF LINEARITY AND NOISE FIGURE OF DIFFERENTIAL COMMON GATE LNA

2.1. Improvement of Linearity of the LNA

The LNA, shown in Fig. 1, comprises a CG stage for the wide input matching, a current source, and a load stage for the wide flat gain. The current source blocks leakage of the RF input signal and adjusts the DC bias current. Even though the load and current source can generate the some distortions, the main source of nonlinearity in the DCG LNA is the CG stage [17]. If the body effect of the CG stage is neglected, the harmonics in the CG stage are generated from g_m (transconductance) nonlinearity, which can be expressed by a Taylor series expansion as follows [18–20].

$$g_m = g_{m1} + g_{m2}v_{gs}^1 + g_{m3}v_{gs}^2 + \dots \quad (1)$$

The corresponding drain current is described as a function of g_m (transconductance) and gate-to-source voltage (v_{gs}).

$$i_d(t) = g_{m1}v_{gs}(t) + g_{m2}v_{gs}^2(t) + g_{m3}v_{gs}^3(t) + \dots \quad (2)$$

The third order harmonic distortion (HD_3) of the DCG LNA is defined as follows [20].

$$HD_3 = \frac{1}{4} \frac{g_{m3}}{g_m} v_{in}^2 \quad (3)$$

In Eq. (3), the coefficient g_{m3} mainly influences the third order distortion. For improving the third order distortion of the CG stage, the negative g_m cell is implemented instead of the current source as shown Fig. 2. It comprised cross-coupled transistors, which generate the negative transconductance ($-g_m$). Therefore, the equivalent model of the half circuit is described as shown Fig. 3, which is composed of

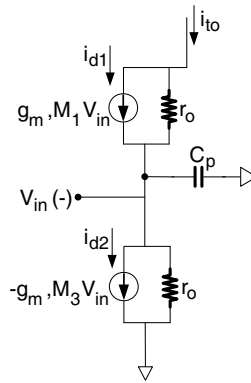


Figure 3. Equivalent model of the half circuit of the proposed LNA.

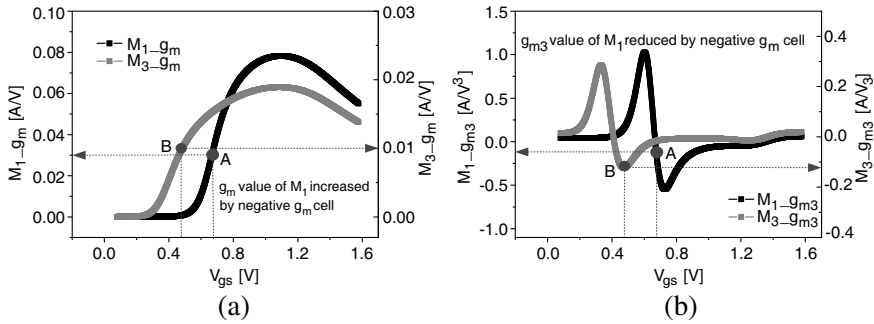


Figure 4. (a) g_m curve of M_1 in the CG stage and M_3 in negative g_m cell, (b) g_{m3} curve of M_1 in the CG stage and M_3 in negative g_m cell.

parallel $1/g_m$ of the CG stage, $-1/g_m$ of the negative g_m cell. The input impedance is given by

$$Z_{in} \approx \frac{1}{g_{m,M1} - g_{m,M3}} \tag{4}$$

and HD_3 of the DCG LNA with the negative g_m cell is defined as follow:

$$HD_3 = \frac{1}{4} \frac{(g_{m3,M1} - g_{m3,M3})}{(g_{m,M1} - g_{m,M3})} v_{in}^2 \tag{5}$$

Since the input impedance and HD_3 are defined by g_m values of M_1 and M_3 cells, it is expected that the g_m distortion can be canceled as well as input is matched by proper design. Figs. 4(a) and (b) show the g_m and g_{m3} values for the M_1 and M_3 transistors. The g_m values of the node A and B in Fig. 4(a) provides to 20 ms for 50Ω match. Since the g_{m3}

$V_{n,c}$ across the source input impedance [22, 24].

$$V_{n,c} = I_n R_s \tag{6}$$

$V_{n,c}$ is amplified by M_4 of the negative g_m cell and delivered to the load, creating the correlation noise ($V_{n,2}$) [16, 25–27].

$$V_{n,2} = -g_{m,M4} I_n R_s R_L \tag{7}$$

Since $V_{n,1}$ and $V_{n,2}$ is differential output, they are calculated as follow.

$$V_{n,out1} = V_{n,2} - V_{n,1} = -g_{m,M4} I_n R_s R_L + I_n R_L = R_L I_n (1 - R_S g_{m,M4}) \tag{8}$$

$V_{n,out1}$ is reduced by a factor of $R_s g_{m,M4}$, which is 0.5 in our design, and the noise figure of the LNA is improved. Table 1 shows the total noise figure and the spectral density of the CG stage with and without the negative g_m cell over the temperature. Although the noises are not reduced exactly to a half due to the other noise sources, the proposed LNA improves the noise figure in the wideband over temperature.

Table 1. Total noise figure and noise contribution of the CG stage with and without the negative g_m cell over temperature.

Temperature [°C]	MHz	With the negative g_m cell		Without the negative g_m cell	
		[V ² / Hz]	Total NF [dB]	[V ² / Hz]	Total NF [dB]
-20	900 MHz	1.26e-18	2.97	1.62e-18	3.27
	1300 MHz	1.06e-18	2.70	1.44e-18	3.03
	1800 MHz	0.94e-18	2.46	1.3e-18	2.78
	2400MHz	0.94e-18	2.2	1.5e-18	2.52
	3000 MHz	1.16e-18	2.0	1.5e-18	2.36
	3200 MHz	1.18e-18	2.0	1.92e-18	2.35
25	900 MHz	1.51e-18	3.3	1.92e-18	3.9
	1300 MHz	1.48e-18	3.1	1.9e-18	3.7
	1800 MHz	1.24e-18	2.8	1.7e-18	3.3
	2400MHz	1.26e-18	2.5	1.7e-18	3.0
	3000 MHz	1.47e-18	2.3	1.89e-18	2.8
	3200 MHz	1.64e-18	2.37	1.92e-18	2.87
85	900 MHz	1.94e-18	3.8	2.36e-18	4.4
	1300 MHz	1.78e-18	3.5	2.3e-18	4.2
	1800 MHz	1.68e-18	3.2	2.15e-18	3.8
	2400MHz	1.68e-18	2.9	2.1e-18	3.4
	3000 MHz	1.92e-18	2.7	2.2e-18	3.2
	3200 MHz	1.92e-18	2.7	2.2e-18	3.2

Reduction of Spectral density

3. REALIZATION AND MEASURED RESULTS

We have designed the wideband LNA with the negative g_m cell. A prototype of this LNA has been fabricated in a $0.13\ \mu\text{m}$ RF CMOS process. The die micrograph is shown in Fig. 7 and the core chip area without pads is $0.57 \times 0.6\ \text{mm}^2$, whose size can be reduced further by proper layout. To test the chips, an evaluation chip board is fabricated using an FR-4 printed circuit board (PCB) and the chip is directly mounted on the ground plane of the evaluation chip board. The width/length of the common gate stage cell are $134.4\ \mu\text{m}/0.13\ \mu\text{m}$ and the negative g_m cell is $26\ \mu\text{m}/0.4\ \mu\text{m}$, respectively. The load resistance is $220\ \Omega$ and the load inductor is $10\ \text{nH}$ for the wide impedance. For a single-ended signal into the differential signal, off-chip baluns at 0.9 , 1.3 , 1.8 , 2.4 , and $3.2\ \text{GHz}$ center frequencies with $100\ \text{MHz}$ bandwidth are employed. The simulation of S_{11} and S_{22} are depicted in Fig. 8 and the stability factor shows in Fig. 9. The measured and simulated power gains are about $14.5\ \text{dB}$ from $700\ \text{MHz}$ to $3500\ \text{MHz}$ as shown in Fig. 10.

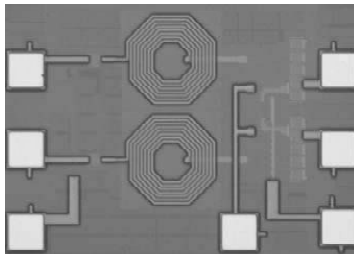


Figure 7. Photograph of proposed wideband LNA: chip size of the LNA with pads ($1 \times 1\ \text{mm}^2$), without pads ($0.57 \times 0.6\ \text{mm}^2$).

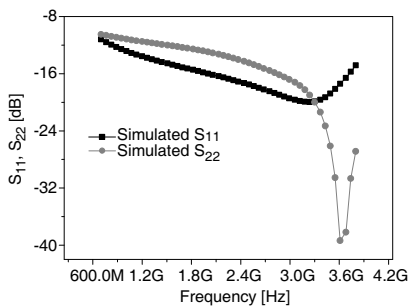


Figure 8. Simulated S_{11} and S_{22} .

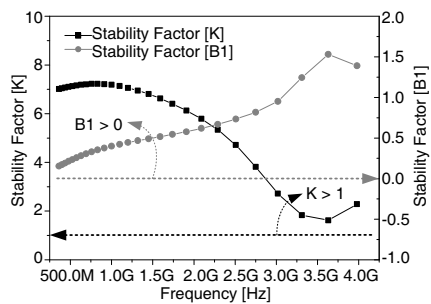


Figure 9. Simulated stability factor (K and B_1 factor).

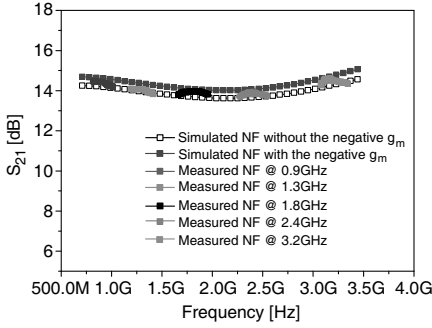


Figure 10. Measured and simulated power gains.

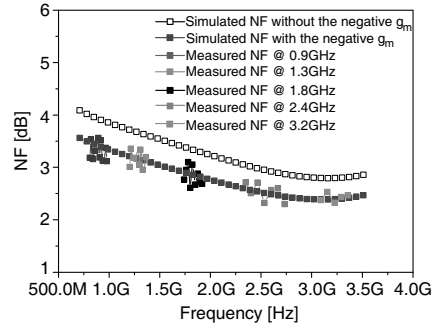


Figure 11. Measured and simulated noise figures.

Table 2. Measured performance compared with prior published the differential Wideband LNAs

* : This work specifies the IIP3 and NF in the wideband.

◇ : This work is the simulation results.

• : The chip sizes are the without pads.

	This work	[14]	[16] [◇]	[26]	[27]
Technology (μm)	0.13	0.18	0.13	0.13	0.5
Bandwidth (GHz)	0.7–3.5	1.2–11.9	0.2–3.8	0.1–0.93	0.8–0.95
S_{11} (dB)	< -10	< -11	< -10	< -10	-
S_{21} (dB)	14–15.4	9.7	11.2	13	12.2
IIP3* (dBm)	4.0–6.0	-6.2	-2.7	-10.2	6.7
NF* (dB)	2.3–3.8	4.5–5.1	2.55–2.85	4.0	3.0
Power (mW)	4.5	20	1.9	0.72	27
Chip sizes [•] (mm ²)	0.342	0.59	-	0.2679	0.2

The noise figure is depicted in Fig. 11, which shows under 3.8 dB across the band. The simulated noise figure of the DCG LNA with the negative g_m cell is improved about 0.6 dB compared to that without the negative g_m cell. To measure the linearity, a two-tone test is performed at 1 MHz offsets from 0.9, 1.3, 1.8, 2.4, and 3.2 GHz frequencies. We apply V_{DD} of 1.5 V and the total current consumes 3 mA. Fig. 12 shows the fundamental and third order harmonic frequency voltages as a function of the differential RF input power swing. The measured

IIP3 is 6.6 dBm at 0.9 GHz, 6.0 dBm at 1.3 GHz, 4.0 dBm at 1.8 GHz, 4.8 dBm at 2.4 GHz, and 4.3 dBm at 3.2 GHz respectively. These measured data are summarized in Table 2 and compared with prior published works.

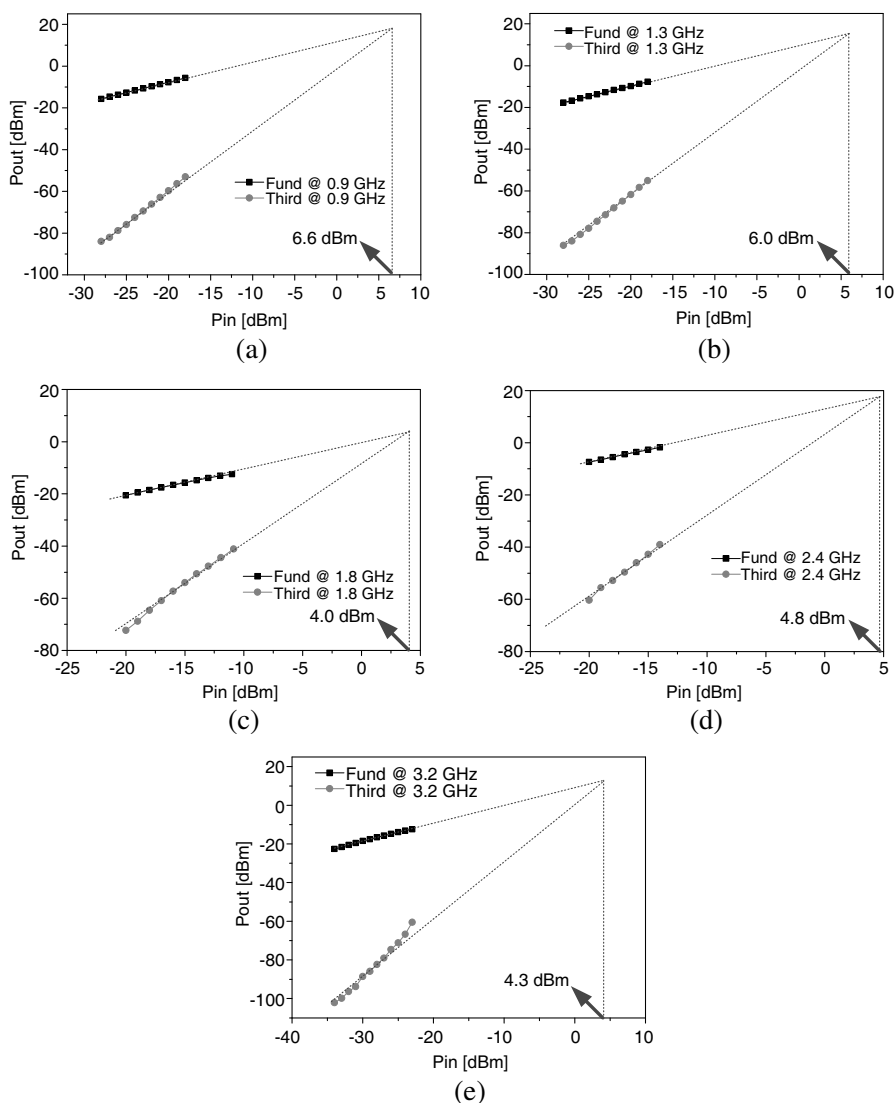


Figure 12. Measured results of the fundamental and third order harmonic powers.

4. CONCLUSIONS

We have designed a differential common gate LNA with the negative g_m cell for wideband application. The CG stage has poor noise figure as well as poor linearity. To improve the performances across a wide bandwidth, using the negative g_m cell is employed instead of the current source. The input admittance are parallel circuit of g_m of common gate stage and $-g_m$ of negative g_m cell. By adjusting the two g_m 's, the third harmonic can be canceled, while input is matched across the band. The harmonics from the CG stage is canceled by the negative phase harmonic generated from the negative g_m cell. The noise from CG stage is amplified by the negative g_m cell and delivered to the opposite terminal, making the noise canceling. Therefore, the LNA can deliver the improved linearity and noise performance.

ACKNOWLEDGMENT

This work was supported by WCU (World Class University) program through the Korea Science and Engineering Foundation funded by the Ministry of Education, Science and Technology (Project No. R31-2008-000-10100-0), and by the Center for Advanced Transceiver Systems, which was sponsored by the nextgeneration new technology development programs of the Ministry of Knowledge and Economy (MKE).

REFERENCES

1. Statszewski, R. B., et al., "All-digital TX frequency synthesizer and discrete-time receiver for bluetooth radio in 130-nm CMOS," *IEEE Journal of Solid-stage Circuits*, Vol. 39, 2278–2291, Dec. 2004.
2. Bagheri, R., A. Mirzaei, S. Chehrazi, M. E. Heidari, M. Lee, M. Mikhemar, W. Tang, and A. A. Abidi, "An 800-MHz–6-GHz software-defined wireless receiver in 90-nm CMOS," *IEEE Journal of Solid-stage Circuits*, Vol. 41, 2860–2874, Dec. 2006.
3. Ismail, A. and A. A. Abidi, "A 3–10-GHz low-noise amplifier with wideband LC-ladder matching network," *IEEE Journal of Solid-Stage Circuits*, Vol. 39, No. 12, 2269–2277, Dec. 2004.
4. Yu, X. and G.-G. Bi, "Performance of multiband complex wavelet based multicarrier Ds-CDMA system with multi-antenna receiver over Nakagami-M fading channel," *Progress In Electromagnetics Research*, PIER 98, 251–266, 2009.

5. Wang, Z., P. Li, R.-M. Xu, and W. Lin, "A compact X-band receiver front-end module based on low temperature co-fired ceramic technology," *Progress In Electromagnetics Research*, PIER 92, 167–180, 2009.
6. Kim, J.-H., Y.-H. You, K.-I. Lee, and J.-H. Yi, "Pilot-less synchronization receiver for UWB-based wireless application," *Progress In Electromagnetics Research*, PIER 83, 119–131, 2008.
7. Hashemi, H. and A. Hajimiri, "Concurrent multiband low-noise amplifiers-theory, design, and applications," *IEEE Transactions on Microwave Theory and Techniques*, Vol. 50, 288–301, Jan. 2002.
8. Ramzan, R., S. Andersson, J. Dabrowski, and C. Svensson, "A 1.4 V 25 mW inductorless wideband LNA in 0.13 μm CMOS," *ISSCC Dig. Tech. Papers*, 424–425, Feb. 2007.
9. Khalaj-Amirhosseini, M., "Wideband or multiband complex impedance matching using microstrip nonuniform transmission lines," *Progress In Electromagnetics Research*, PIER 66, 15–25, 2006.
10. Girlando, G. and G. Palmisano, "Noise figure and impedance matching in RF cascode amplifiers," *IEEE Trans. Circuits and Syst. II: Analog Digit. Signal Process*, Vol. 46, 1388–1396, Nov. 1999.
11. Azmi, P. and N. Tavakkoli, "Narrow-band interference suppression in CDMA spread-spectrum communication systems using pre-processing based techniques in transform-domain," *Progress In Electromagnetics Research Letters*, Vol. 3, 141–150, 2008.
12. Kim, T. W., "A common-gate amplifier with transconductance nonlinearity cancellation and its high-frequency analysis using the volterra series," *IEEE Transactions on Microwave Theory and Techniques*, Vol. 51, No. 5, 1461–1469, Jun. 2009.
13. Ponnekanti, S. and S. Sali, "Non-linear interference cancellation techniques for electromagnetically dense propagation environments," *Progress In Electromagnetics Research*, PIER 18, 209–228, 1998.
14. Liao, C.-F. and S.-I. Liu, "A broadband noise-canceling CMOS LNA for 3.1-10.6-GHz UWB receivers," *IEEE Journal of Solid-state Circuits*, Vol. 42, No. 2, 329–338, Feb. 2007.
15. Blaakmeer, S. C., E. A. M. Klumperink, D. M. W. Leenaerts, and B. Nauta, "Wideband balun-LNA with simultaneous output balancing, noise-canceling and distortion-canceling," *IEEE Journal of Solid-state Circuits*, Vol. 43, No. 6, 1341–1350, Jun. 2008.

16. Amer, A., E. Hegazi, and H. F. Ragaie, "A 90-nm wideband merged CMOS LNA and mixer exploiting noise cancellation," *IEEE Journal of Solid-state Circuits*, Vol. 42, No. 2, 323–328, Feb. 2007.
17. Razavi, B., *RF Microelectronics*, Prentice Hall, 1998.
18. Zhang, J., J.-Z. Gu, B. Cui, and X.-W. Sun, "Compact and harmonic suppression open-loop resonator bandpass filter with tri-section sir," *Progress In Electromagnetics Research*, PIER 69, 93–100, 2007.
19. Kang, J., J. Yoon, K. Min, D. Yu, J. Nam, Y. Yang, and B. Kim, "A highly linear and efficient differential CMOS power amplifier with harmonic control," *IEEE Journal of Solid-state Circuits*, Vol. 41, No. 6, 1314–1322, Jun. 2006.
20. Khalaj-Amirhosseini, M., "Analysis of periodic and aperiodic coupled nonuniform transmission lines using the Fourier series expansion," *Progress In Electromagnetics Research*, PIER 65, 15–26, 2006.
21. Shaeffer, D. K. and T. H. Lee, "A 1.5-V, 1.5-GHz CMOS low noise amplifier," *IEEE Journal of Solid-state Circuits*, Vol. 32, No. 5, 745–759, May 1997.
22. Deen, M. J. and T. A. Fkeldly, *CMOS RF Modeling, Characterization and Applications*, World Scientific, 2002.
23. Bevilacqua, A. and A. M. Niknejad, "An ultra-wideband CMOS LNA for 3.1 to 10.6 GHz wireless receivers," *ISSCC Dig. Tech. Papers*, 382–383, Feb. 2004.
24. Orimoto, H. and A. Ikuta, "Signal processing for noise cancellation in actual electromagnetic environment," *Progress In Electromagnetics Research*, PIER 99, 307–322, 2009.
25. Bruccoleri, F., et al., "Noise cancelling in wideband CMOS LNAs," *ISSCC Dig. Tech. Papers*, Vol. 1, 406–407, May 2002.
26. Wang, S. B. T., A. M. Niknejad, and R. W. Brodersen, "Design of a sub-mW 960-MHz UWB CMOS LNA," *IEEE Journal of Solid-state Circuits*, Vol. 41, 2449–2456, Nov. 2006.
27. Zhuo, W., S. Embabi, J. P. De Gyvez, and E. Sanchez-Sinencio, "Using capacitive cross-coupling technique in RF low noise amplifiers and down-conversion mixer design," *Proc. ESSCIRC*, 116–119, 2000.